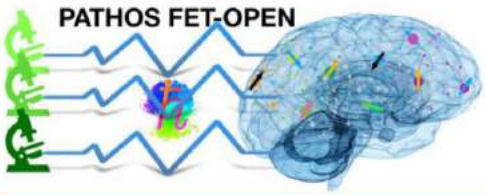

PHOTONIC AND NANOMETRIC HIGH-SENSITIVITY BIO-SENSING

Deliverable D2.2 [INRIM M42]
Paper demonstrating advantage of ZD protocols in specific optical measurements procedures
Partners involved: INRIM, UNIFI, WEIZMANN

We illustrate the results obtained with the first experimental demonstration of a noise diagnostics technique based on repeated quantum measurements. We establish the ability of a single photon, undergoing random polarisation noise, to estimate non-Markovian temporal correlations within such a noise by means of frequent, (partially-)selective polarization measurements. We show how a noise characterized by positive (negative) temporal correlations corresponds to our single photon undergoing a dynamical regime enabled by the quantum Zeno (anti-Zeno) effect. This can be regarded as the first step towards a novel kind of noise spectroscopy based on quantum (anti-)Zeno effect in single-photon state probing, able to extract information on the noise while protecting the probe state, a conceptual paradigm shift with respect to traditional interferometric noise spectroscopy techniques.

Introduction. Quantum control [1, 2] is a fundamental tool for developing highly accurate quantum technologies. In particular, the quantum Zeno (QZE) [3–8] and anti-Zeno (AZE) [7–11] effects, respectively denoting the slowdown and speedup of quantum system evolution by its frequent interruptions [12–20], have been recognised (beyond their fundamental significance) as general paradigms of quantum control [21–26]. Indeed, they allow either protecting [27–29] or steering [30, 31] the quantum state of a system via an interplay between the effects of frequent operations (system control) and the coupling of the system to its environment (a bath) [22, 32–35].

These paradigms generality is revealed by the Kofman-Kurizki (KK) universal formula, whereby the overlap of the system-bath coupling spectrum with the system-control spectrum determines the initial-state population decay (relaxation) rate $\gamma(t)$ [9, 22, 33, 34]

$$\gamma(t) = 2\pi \int_{-\infty}^{\infty} d\omega\, G(\omega) F_t(\omega), \tag{1}$$

$G(\omega)$ being the system-bath coupling spectrum (bath response) and $F_t(\omega)$ the system-control spectrum evaluated within the time interval $[0, t]$. According to Eq. (1), the QZE (AZE) corresponds to the suppression (enhancement) of the bath-induced decay $\gamma(t)$ by the reduction (increase) of the overlap between the chosen $F_t(\omega)$ and the bath response $G(\omega)$ [9, 22] (see Supplemental Material for details). This means that the time-variation of the system control must be much faster than (for QZE) or as fast as (for AZE) the bath correlation time, with the result that both effects are distinctly non-Markovian. Overall, the only condition on Eq. (1) validity is the weakness of the system-bath coupling, allowing for a perturbative treatment of the bath effects. The KK formula has been confirmed in scenarios involving frequent perturbations of open-system evolution, e.g., cold atoms dynamics in optical lattices [12, 22], light propagation in waveguides and cavities [5, 36], AZE-cooling and QZE-heating of qubits coupled to a bath [37, 38]. Moreover, Eq. (1) can be used for designing optimal protection of multi-qubit quantum information processing [39].

In this paper, we study both theoretically and experimentally an alternative purpose of the KK formula, i.e., the diagnostics (characterization) of random processes, alias noise spectroscopy [40]. One may infer the bath-response spectrum $G(\omega)$ upon varying the control spectrum $F_t(\omega)$ and recording the resulting decoherence rate, as experimentally confirmed in [41]. This, however, is a time-consuming process. Alternatively, key information on $G(\omega)$, e.g. its width (the inverse memory time), may be gathered by appropriate dynamical control of the system probing the bath [40]. This represents an innovative and powerful tool that we introduce to expand quantum sensing technology. Although the QZE has been previously used for assisting noise sensing [42, 43], here we demonstrate its ability to extract information on noise processes, a direction not yet investigated and

highly relevant to quantum technologies. More specifically, we demonstrate, for the first time, noise diagnostics by repeated quantum measurements, establishing the ability of a single photon undergoing random polarisation fluctuations to diagnose non-Markovian temporal correlations within this noise. Such a technique becomes crucial especially when extremely faint illumination levels are required, a regime in which traditional methods (e.g., the interferometric ones [44]) are usually ineffective. To do this, we realize the single-photon reservoir spectrum and spectral broadening control proposed in Ref. [32]. In the frequency domain, (non-)Markovian noise correlations correspond, respectively, to (colored) white noise spectra. We show that the noise temporal correlations are diagnosed when the photon undergoes frequent polarisation measurements, demonstrating that positive (negative) correlations give rise to QZE (AZE). This paves the way to a new generation of QZE/AZE-based noise spectroscopy protocols in photon (or other single particle) state probing.

Theoretical model. Consider an iterative procedure in which a single photon, initialised in the horizontally-polarised state $|H\rangle$, passes through a sequence of N blocks at time instants $t_1, \ldots, t_N$. In the k-th block (Fig. 1, $k = 1, ..., N$), the photon

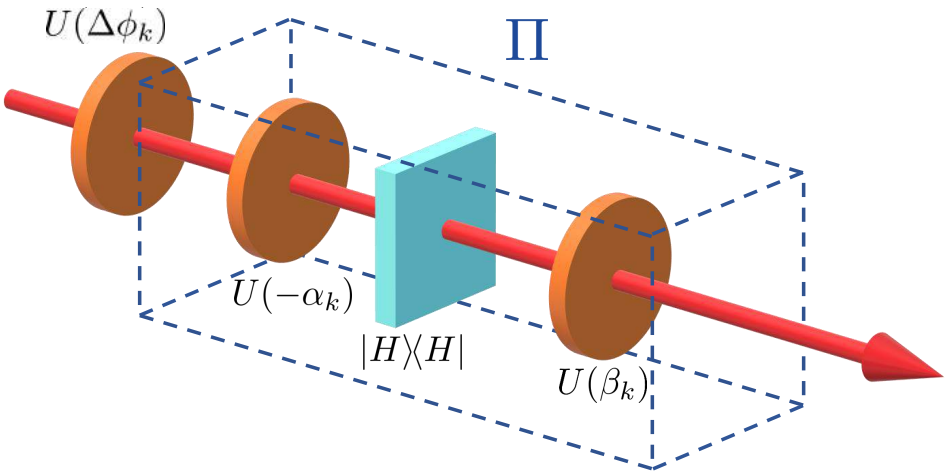

FIG. 1. Scheme of the k-th element in a sequence of N blocks determining the quantum state evolution of a photon passing through them. First, the polarisation state of the photon undergoes a random rotation $U(\Delta\phi_k)$. Then, the unitary rotation $U(-\alpha_k)$, followed by the projection $|H\rangle\langle H|$ and by a proper counter-rotation $U(\beta_k)$, for suitably chosen α_k, β_k (see Supplemental Material for details) reproduces the effect of the selective measurement Π in Eq. (3) at the k-th time instant t_k.

polarisation is rotated by the operator $U(\Delta\phi_k)$, representing a random polarisation rotation in the x-z plane of the Bloch sphere (i.e. a $\hat{\sigma}_y$ Pauli-matrix rotation around the y-axis):

$$U(\Delta\phi_k) = e^{-i\hat{\sigma}_y \Delta\phi_k} = I\cos\Delta\phi_k - i\hat{\sigma}_y \sin\Delta\phi_k, \tag{2}$$

being I the two-dimensional identity matrix. By passing through the N blocks, the horizontal ($|H\rangle$) and vertical ($|V\rangle$) polarisation states evolve as the degenerate states of a two-level system coupled by intermittent polarisation rotations. These rotations are interspersed by an equivalent number of selective measurements, i.e., in each block the photon undergoes a measurement corresponding to partial or complete absorption of the vertical polarisation component (or, equivalently, to partial projection onto the $|H\rangle$ state):

$$\Pi = |H\rangle\langle H| + \theta\,|V\rangle\langle V| = \theta I + (1-\theta)\,|H\rangle\langle H|\,, \tag{3}$$

being $\theta \in [0, 1]$ the parameter determining the measurement selective strength. Such a dynamics can be reproduced with an iterative procedure exploiting, in each block, a k-dependent polarisation rotation $U(-\alpha_k)$ ($k = 1, .., N$), followed by the projection $|H\rangle\langle H|$ and a second (k-dependent) polarisation rotation $U(\beta_k)$. Here, $U(-\alpha_k)$ determines the measurement selective strength on the state entering the k-th block, and $U(\beta_k)$ fixes the polarisation of the outgoing photon. By properly choosing the $\{\alpha_k\}$ and $\{\beta_k\}$ coefficients (see Supplemental Material for details), one can recreate the dynamics induced on the photon polarisation by a sequence of N blocks, each performing a random polarisation rotation $U(\Delta\phi_k)$ followed by the partially-selective projector Π in Eq. (3). Incidentally, this procedure is equivalent, in terms of dynamics, to the scheme proposed in Ref. [32].

The k-th block output is the (unnormalized) state $|\psi(t_k)\rangle = \left(\prod_{l=1}^{k}[\Pi U(\Delta\phi_l)]\right)|H\rangle$. Since the sequence $\Delta\phi_1, \ldots, \Delta\phi_N$ is random, because of the external noise process, we are interested in the horizontal polarisation survival probability averaged over all possible random sequences:

$$\bar{P}_H(t_k) = \overline{|\langle H|\psi(t_k)\rangle|^2}, \tag{4}$$

where the overline denotes the averaging operation.

Consider the case in which polarisation rotation jumps with identical magnitude occur, i.e., $|\Delta\phi_k| = \Delta\phi \; \forall k = 1, ..., N$. We introduce the parameter $\mathcal{C}$ describing the degree of correlation between consecutive jumps, defined as

$$\overline{\Delta\phi}_{\Delta\phi'} = p\Delta\phi' - (1-p)\Delta\phi' = \mathcal{C}\Delta\phi', \tag{5}$$

where $\overline{\Delta\phi}_{\Delta\phi'}$ is the average polarisation rotation jump at the end of the k-th block (provided the previous jump was $\Delta\phi'$) and p denotes the correlation probability between subsequent jumps. Thus, jumps are correlated for $\mathcal{C} > 0$ ($p > 0.5$), anti-correlated for $\mathcal{C} < 0$ ($p < 0.5$), and uncorrelated for $\mathcal{C} = 0$ ($p = 0.5$). Although a universal closed-form solution for the average survival probability in Eq. (4) is not available, an analytical description of all the cases of interest will follow.

Non-random evolution. In the maximally-correlated case $\mathcal{C} = 1$, the time dependence of the survival probability $\bar{P}_H(t_k)$ is the same as for the non-random evolution with identical jumps $\Delta\phi$ or $(-\Delta\phi)$ in each block. In particular, $\forall\theta$ the probability of observing a horizontally-polarised photon becomes [32]:

$$\bar{P}_H(t_k) = \frac{[\lambda_+^k(\cos\Delta\phi - \lambda_-) + \lambda_-^k(\lambda_+ - \cos\Delta\phi)]^2}{(1+\theta)^2\cos^2\Delta\phi - 4\theta}, \tag{6}$$

where $\lambda_\pm \equiv \frac{1}{2}\left[(1+\theta)\cos\Delta\phi \pm \sqrt{(1+\theta)^2\cos^2\Delta\phi - 4\theta}\right]$. In the absence of measurements ($\theta = 1$), one gets $\bar{P}_H(t_k) = \cos^2(k\Delta\phi)$, analogous to Rabi oscillations of the horizontal polarisation probability as a function of the number of blocks (k) traversed by the photon. The opposite limit, $\theta = 0$,corresponds to the *selective* (projective) measurement case, since each time a photon passes through one of the blocks in Fig. 1 its polarisation state is projected onto the horizontal one. Here we have $\bar{P}_H(t_k) = \cos^{2k}(\Delta\phi)$, insensitive to jump sign fluctuations and hence identical for random and non-random evolution, becoming $\bar{P}_H(t_k) = e^{-k(\Delta\phi)^2}$ for small rotation angles ($\Delta\phi \ll 1$). This decay is slower than the period of uninterrupted Rabi oscillations, implying that QZE occurs. Next, consider non-random evolution with $0 < \theta < 1$, corresponding to partially-selective measurements [45]. For small rotation angles and sufficient selective strength ($\Delta\phi \ll 1-\theta$), Eq. (6) reduces to the exponential decay $\bar{P}_H(t_k) = \exp\left[-\frac{(\Delta\phi)^2}{\tau^2\nu}t_k\right]$, with $\nu \equiv \frac{1-\theta}{1+\theta}\frac{1}{\tau}$ and the N blocks assumed to be equidistant ($t_k = k\tau$, being τ the photon flight time between consecutive blocks). The quantity ν is the (effective) measurement rate, i.e., the reciprocal time during which state selection occurs, scaling as $1/\tau$ and decreasing as θ increases. The decay rate diminishes with ν, highlighting the QZE.

Random evolution. Now, consider the case of random noisy modulation of the polarisation rotation $U(\Delta\phi)$ for (anti-)correlated noise ($-1 \leq \mathcal{C} < 1$). In our case of interest, i.e., $\Delta\phi \ll 1$, one has ($\forall\theta$) [32]

$$\bar{P}_H(t_k) = e^{-(\gamma+\Gamma_0)t_k}\left(\cosh(St_k) + \frac{\Gamma_0}{S}\sinh(St_k)\right), \tag{7}$$

where $S \equiv \sqrt{\gamma^2 + \Gamma_0^2}$, $\gamma \equiv \frac{1+\mathcal{C}\theta}{1-\mathcal{C}\theta}\frac{\Delta\phi^2}{\tau}$ is the polarisation decay rate, and $\Gamma_0 \equiv -\frac{\ln\theta}{2\tau}$ denotes the time-averaged rate of photons absorbed by the polarisers (see Supplemental Material for details).

In the absence of measurement ($\theta = 1$), Eq. (7) yields

$$\bar{P}_H(t_k) = \frac{1 + e^{-2\gamma_0 t_k}}{2} \qquad \left(\gamma_0 \equiv \gamma|_{\theta=1}\right) \; . \tag{8}$$

Thus, random polarisation fluctuations lead to complete unpolarisation, i.e., $\bar{P}_H(t) \to 1/2$ for $t \to \infty$.

For weakly-selective measurements ($\theta \to 1$), in the limit $\Gamma_0 \ll \gamma$ Eq. (7) becomes

$$\bar{P}_H(t_k) \approx e^{-\gamma t_k}, \tag{9}$$

showing an exponential decay over time of the horizontal polarisation probability.

Finally, in the projective measurement scenario ($\theta \to 0$), $\bar{P}_H(t_k)$ evolves following Eq. (9), with $\gamma \to \Delta\phi^2/\tau$.

Experimental results. In our setup (Fig. 2), heralded single photons at 702 nm are generated by type-I parametric down-conversion, collected by a single-mode optical fibre and collimated in a Gaussian beam (2 mm width) over a 2m-long path. Each heralded photon, initialised in the horizontal polarisation state $|H\rangle$, traverses $N = 7$ stages composed of a half-wave plate (HWP) and a polariser, reproducing the dynamics of a sequence of $N = 7$ blocks in Fig. 1. In the k-th stage, the HWP is responsible for the combined effect of the global rotation $U(\alpha_k)U(\Delta\phi_k)U(\beta_{k-1})$. The polariser, instead, realises the projector $|H\rangle\langle H|$. Each stage induces a random polarisation rotation jump $\pm\Delta\phi$ (selected by a random number generator, with $\Delta\phi = 4^\circ$) and realises the (partially) selective measurement Π in Eq. (3). Each jump is set to be equal (correlated) to the one in the previous

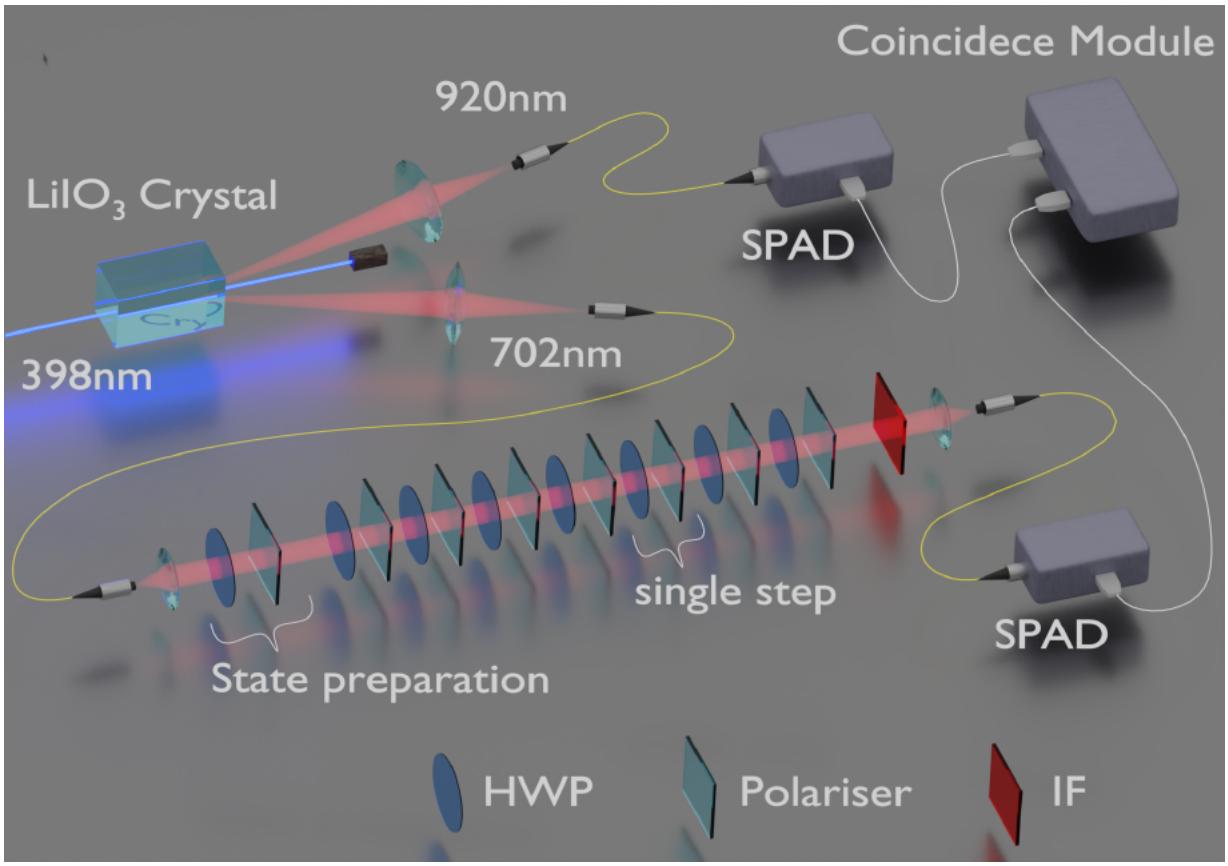

FIG. 2. Heralded single photons at 702 nm are fibre-coupled and then collimated in a Gaussian beam. After being prepared in the $|H\rangle$ state by a polariser, each photon passes through a series of $N = 7$ polarization rotation/measurement stages. When Zeno measurements occur, each stage hosts a half-wave plate (HWP) and a polarizer, while in the absence of measurements only a HWP is present (after the N-th stage, a polarizer performs the final projection $|H\rangle\langle H|$). An interference filter (IF, 3 nm FWHM) removes environmental light, then the photons are fibre-coupled and detected by a silicon single-photon avalanche diode (SPAD).

block with probability $p = \frac{\mathcal{C}+1}{2}$. At the end of the sequence, only horizontally-polarised photons are detected. We have three possible handles on the photon detection probability: (i) the parameter θ, determining the selective strength of the measurement Π in Eq. (3); (ii) the correlation coefficient $\mathcal{C}$; (iii) the polarization jump amplitude $\Delta\phi$. In the experiment we have investigated three cases, $\mathcal{C} = -0.6$, 0 and 0.4, whilst varying θ and keeping $\Delta\phi = 4^\circ$. For each $\mathcal{C}$ value, we have measured the single-photon detection probabilities and standard deviations (uncertainties) of 100 random sequences of $N = 7$ jumps. Fig. 3 presents the behavior of the photon detection probability with time (i.e., with respect to t_k) in two different regimes: $\theta = 0$, corresponding to a projective measurement, and $\theta = 1$, i.e. in the absence of measurement (the measurement strength decreases as θ increases). Fig. 4, instead, shows the results obtained for an intermediate selective strength $0 < \theta < 1$, i.e. from the projective measurement limit to the weakly-selective measurement one. In the case Markovian case $\mathcal{C} = 0$, the measured probability is independent of θ. The novel, hitherto unobserved result is that for $\mathcal{C} > 0$ ($\mathcal{C} < 0$) the QZE (AZE) is revealed, meaning slowdown (speedup) of the decay compared to the uncorrelated case. By varying θ, one can promote or suppress both effects [32, 46, 47]. In both Figs. 3 and 4, the obtained results (dots) are in good agreement, within the experimental uncertainties, with the theoretical predictions (lines).

Finally, for each noise (anti-)correlation regime investigated we tried to estimate the correlation parameter $\mathcal{C}$ by comparing the $\bar{P}_H$ value at the end of our process (i.e., at the time instant t_7) with and without Zeno measurements ($\bar{P}_H^{(\theta=0)}$ and $\bar{P}_H^{(\theta=1)}$, respectively). By interpolating the results of numerical simulations based on Eq. (4) we can extract the behavior of $\mathcal{C}$ with respect to the differential average probability $\Delta\bar{P}_H = \bar{P}_H^{(\theta=0)} - \bar{P}_H^{(\theta=1)}$, reported as a blue line in Fig. 5. From the experimental $\Delta\bar{P}_H$ values and uncertainties (orange dashed and solid lines, respectively) obtained for each $\mathcal{C}$ theoretical value (highlighted by the black dots on the Y axis), we can estimate the corresponding experimental value $\mathcal{C}^{(exp)}$, indicated by a green dashed line. For each regime investigated, the green solid lines delimit the confidence interval $\mathcal{I}_\mathcal{C}$ on $\mathcal{C}^{(exp)}$, obtained propagating the experimental uncertainty on $\Delta\bar{P}_H$ and reported in the inset table together with $\mathcal{C}^{(exp)}$ and the theoretical prediction $\mathcal{C}^{(th)}$.

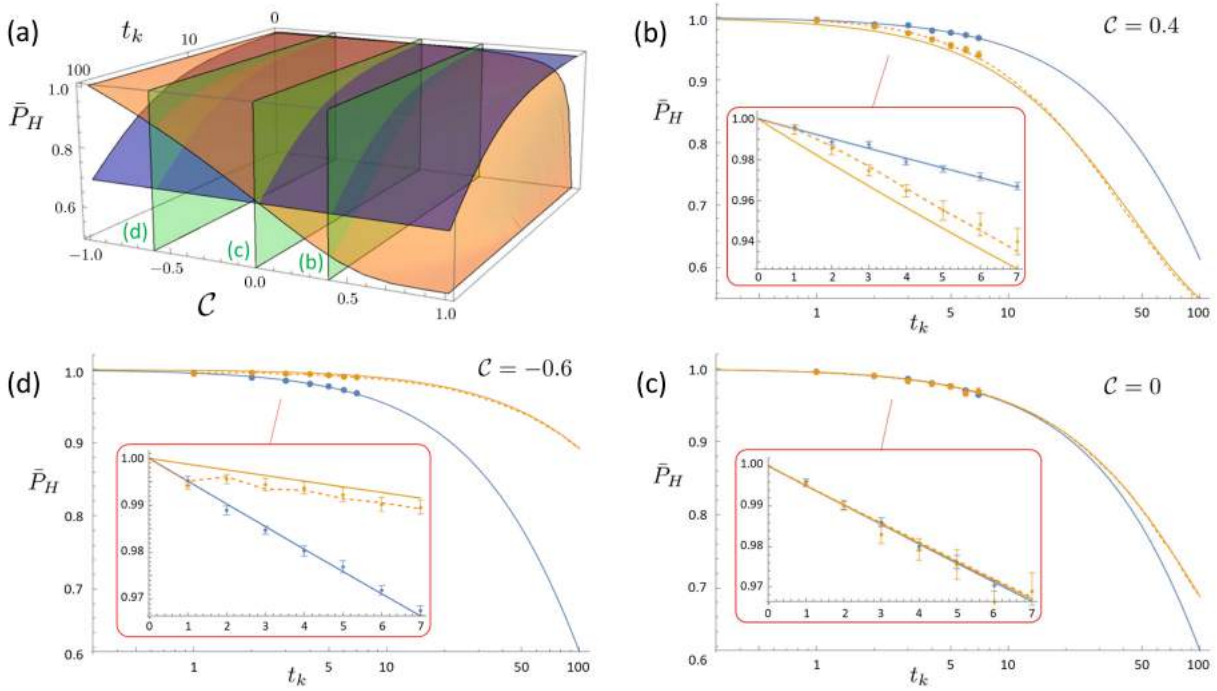

FIG. 3. QZE (AZE) effect as a signature of (anti-)correlated noise. Panel (a): theoretical average probability $\bar{P}_H(t_k)$ to detect a horizontally-polarised single photon for (anti-)correlated consecutive jumps of magnitude $\Delta\phi = 4^\circ$, as a function of t_k and the noise correlation parameter $\mathcal{C}$, in presence ($\theta = 0$, blue surface) and absence ($\theta = 1$, orange surface) of measurement. The green planes indicate the $\mathcal{C}$ values considered in our experiment, whose results are shown in panels (b)-(d).There, the experimental data are shown for both $\theta = 1$ (no measurement, in orange) and $\theta = 0$ (projective measurement, in blue), with the statistical uncertainties evaluated as the standard deviation of 100 different realisations. The solid curves show the theoretical predictions, given by Eqs. (8) and (9), respectively. The dashed orange lines show, instead, $\bar{P}_H(t_k)$ numerical estimations for $\theta = 1$, as per Eq. (4), obtained by averaging over 100 simulated random sequences of $\pm\Delta\phi$ jumps. The inset plots (red boxes) show the detail of the experimentally-investigated region $t_k \in [0, 7]$.

All the estimated values are in good agreement with their theoretical counterparts, certifying the reliability and robustness of our single-photon technique for quantum noise correlations estimation.

Up to now, we limited our considerations to linear polarization rotations (of fixed magnitude) around a fixed axis. Nonetheless, our method can be extended to very general classes of noise. For this purpose, we performed numerical simulations considering a generic unitary polarization noise model, i.e. a polarization jump with random amplitude along a generic, randomly chosen axis of the Bloch sphere. The results of this systematic study, shown in detail in the Supplemental Material, demonstrate that the same behavior as in our proof-of-principle experiment can be observed also in this case, indicating that a quantitative estimation of the correlation parameter $\mathcal{C}$ might be possible. Anyway, the precise experimental implementation of our technique in this scenario is demanded to further studies, as well as the investigation of methods for increasing the number of steps realized, eventually following the line of Ref. [48].

Conclusions. We have experimentally investigated the loss of polarisation coherence of a single photon undergoing stochastic polarisation noise (polarisation rotation jumps) and, concurrently, frequent (weak or strong) selective quantum measurements, demonstrating that the polarisation decay rate depends on non-Markovian correlations within the noise. More specifically, the key feature is that correlated jumps give rise to decay-rate slowdown (QZE), while anti-correlated ones to its speedup (AZE), fully complying with the KK universal formula for the decay-rate dependence on the overlap between the noise and frequent-measurement spectra [9, 22, 34]. This demonstration enables the use of photons and other particles as hitherto unexplored probes of noise correlations. As shown above, a limited number (here, 100) of single-photon polarisation coherence loss events in a noisy medium probed by a few (here, $N = 7$) selective measurements can reveal unequivocally the noise correlation characteristics. Characterizing noise, especially in non-Markovian processes [49–51], is a very important tool for several quantum technologies. To this end, the present scheme may be modified by inserting a fluctuating birefringent medium between consecutive measurements [28], thereby allowing the sensing [40] of the polarisation noise spectrum associated with a propagating photon.

Among the envisaged applications of the proposed noise sensing method we may contemplate, e.g., the probing of magnetic field fluctuations, that can be translated into photon polarization fluctuations through the Faraday effect [52–55]. Single-photon

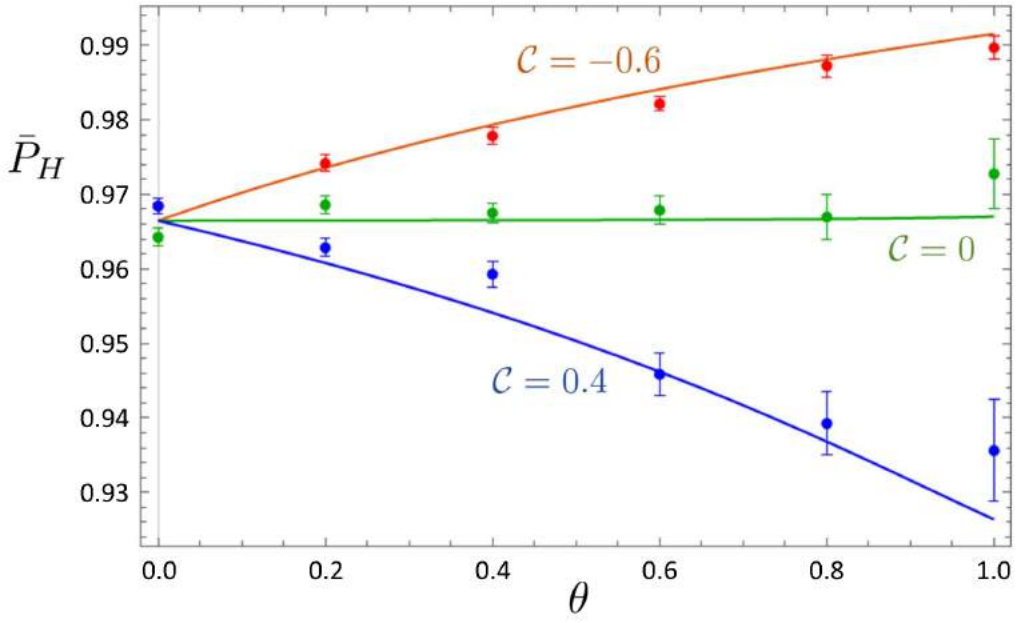

FIG. 4. Average probability $\bar{P}_H(t_7)$ to detect a horizontally-polarised single photon at the end of our protocol, as a function of the selective strength θ of the measurement Π in Eq. (3), for the three $\mathcal{C}$ values chosen for our experiment. The lines represent the theoretical predictions given by Eq. (7) for $\tau = 1$ and $k = 7$, while the dots show the measured $\bar{P}_H(t_7)$ for different θ values. Experimental uncertainties are evaluated as the standard deviation of the 100 different realisations results.

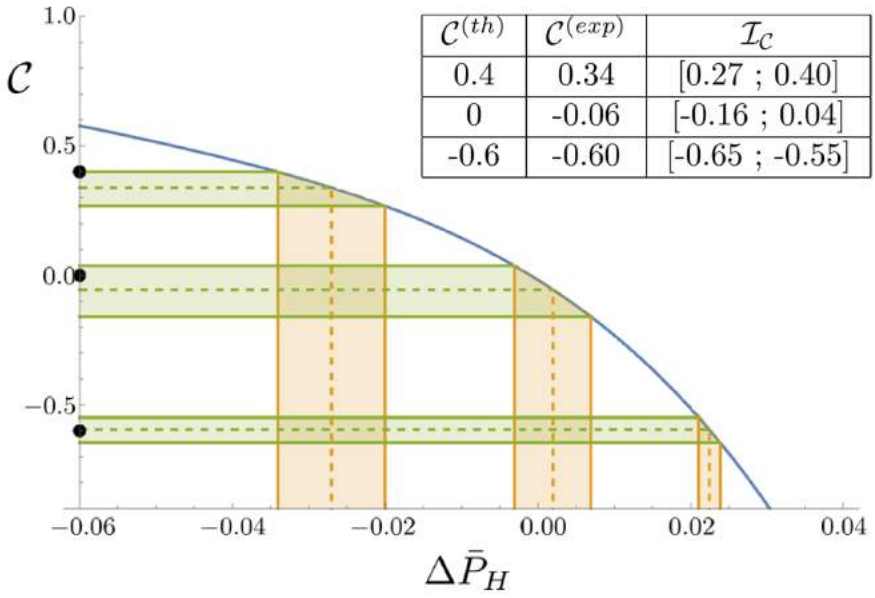

$\mathcal{C}^{(th)}$	$\mathcal{C}^{(exp)}$	$\mathcal{I}_\mathcal{C}$
0.4	0.34	[0.27 ; 0.40]
0	-0.06	[-0.16 ; 0.04]
-0.6	-0.60	[-0.65 ; -0.55]

FIG. 5. Estimation of the noise correlation parameter $\mathcal{C}$ from the differential average probability $\Delta\bar{P}_H = \bar{P}_H^{(\theta=0)} - \bar{P}_H^{(\theta=1)}$, being $\bar{P}_H^{(\theta=0)}$ and $\bar{P}_H^{(\theta=1)}$ the average probabilities of detecting a horizontally-polarised photon at the end of our protocol with or without Zeno measurements, respectively. The blue line shows the dependence of $\mathcal{C}$ on $\Delta\bar{P}_H$, obtained from numerical simulations based on Eq. (4). The orange dashed (solid) lines represent the experimental $\Delta\bar{P}_H$ values (uncertainties) for each regime investigated ($\mathcal{C} = -0.6$, $\mathcal{C} = 0$ and $\mathcal{C} = 0.4$, indicated by the black dots on the Y axis). The green dashed and solid lines indicate instead, respectively, the corresponding $\mathcal{C}$ values and associated 1σ confidence intervals (being σ the uncertainty on the measured $\Delta\bar{P}_H$). The inset table shows the extracted $\mathcal{C}^{(exp)}$ values, together with the associated confidence intervals $\mathcal{I}_\mathcal{C}$ (obtained by propagating the uncertainties on $\Delta\bar{P}_H$), compared with their theoretical counterpart $\mathcal{C}^{(th)}$.

probing of such fluctuations may be used to explore vacuum magnetic birefringence [56], parity violation in atoms [57] and weak-magnetic-noise calibration [58]. Further applications conceive disordered media [59] and physiological processes sensing, like polarisation microscopy of birefringent cholesterol crystals in human biological (synovial, pleural and pericardial) fluids

to diagnose rheumatoid diseases [60–62] and atherosclerosis [63]. Finally, a relevant role in protein biosynthesis is played by chirality, allowing for polarisation-based biophysical techniques for protein structure characterisation [64, 65]; combining them with our sensing technique we could open new possibilities to study biopolymer synthesis and evolution, investigating eventual correlations among morphological structures occurring during biochemical processes.
To conclude, we have established the possibility of probing correlations in random fluctuations of photon polarisation by QZE/AZE observation in the polarisation evolution. Our sensing procedure, differently from interferometric measurements [44], works even at extremely low illumination levels, allowing its application to highly photosensitive materials and molecules, when (almost) no photon has to be absorbed by the sample. This paves the way to a whole new kind of quantum sensing techniques, able to extract information on the noise affecting a quantum channel while preserving the probe quantum state.

DYNAMICAL EVOLUTION OF THE PHOTON POLARISATION

Let us analyse in more detail the effects of having noisy modulation of the polarisation rotator. In the case of random evolution ($-1 \leq \mathcal{C} < 1$), for sufficiently small angles $\Delta\phi$, a master equation (ME) can be derived for the evolution of the polarisation probabilities averaged over the realisations of the random process and smoothed over the evolution time [32]. This ME yields the following rate equations for the average probabilities of the two orthogonal polarisations:

$$\begin{aligned} \dot{\bar{P}}_H &= -\gamma \bar{P}_H + \gamma \bar{P}_V, \\ \dot{\bar{P}}_V &= \gamma \bar{P}_H - (\gamma + 2\Gamma_0)\bar{P}_V. \end{aligned} \tag{10}$$

Here, $2\Gamma_0$ is the time-averaged photon absorption rate, with

$$\Gamma_0 = -\ln\theta/\tau, \tag{11}$$

and γ denotes the polarisation decay rate:

$$\gamma = \frac{1+\mathcal{C}\theta}{1-\mathcal{C}\theta}\frac{\Delta\phi^2}{\tau}. \tag{12}$$

The solution of Eqs. (10) for the horizontal component of the photon polarisation is:

$$\bar{P}_H(t) = e^{-(\gamma+\Gamma_0)t}\left(\cosh(St) + \frac{\Gamma_0}{S}\sinh(St)\right), \tag{13}$$

where $S \equiv \sqrt{\gamma^2 + \Gamma_0^2}$. This solution describes the polarisation at the discrete time instants t_k. The validity condition for Eqs. (10)-(13) is $\gamma \ll \nu$, or [32]

$$\langle(\Delta\phi_k)^2\rangle \ll (1-\mathcal{C})(1-\mathcal{C}\theta), \tag{14}$$

i.e., the polarisation rotation jumps distribution variance should be sufficiently small, and $\mathcal{C}$ should not be too close to 1.

POLARISATION DECAY RATE UNDER RANDOM EVOLUTION AND MEASUREMENTS

The polarisation decay rate obeys the universal KK formula [9, 22, 34], but applied to the discrete-time evolution case identified by the finite integration limits $\pm\pi/\tau$, i.e.:

$$\gamma = 2\pi\int_{-\pi/\tau}^{\pi/\tau} d\omega\, G(\omega)F(\omega). \tag{15}$$

Here

$$G(\omega) = \frac{\Delta\phi^2}{2\pi\tau}\frac{1-\mathcal{C}^2}{1+\mathcal{C}^2-2\mathcal{C}\cos\omega\tau} \tag{16}$$

is the spectral density associated with the rotation-angle fluctuations (also called "bath" or "reservoir" spectrum), whereas the measurement control spectrum

$$F(\omega) = \frac{\tau}{2\pi}\frac{1-\theta^2}{1+\theta^2-2\theta\cos\omega\tau} \tag{17}$$

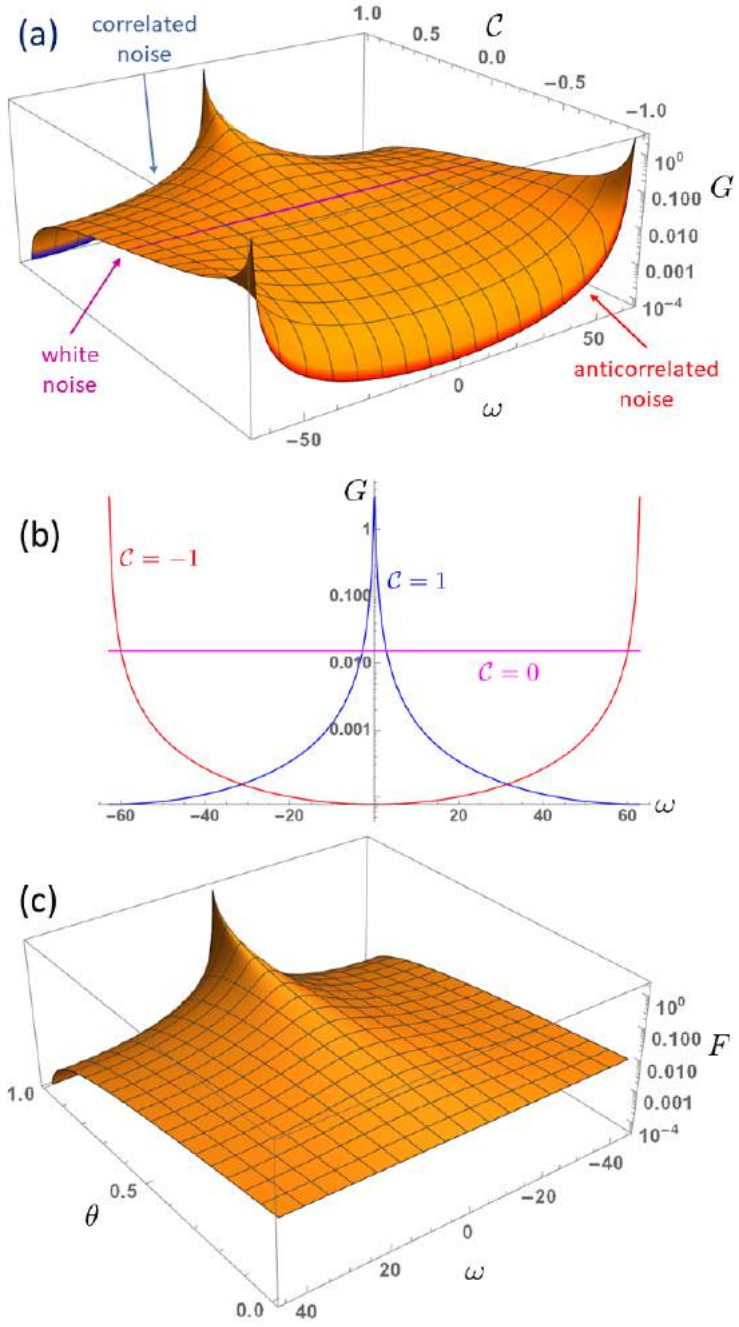

FIG. 6. Plot (a): spectral density $G(\omega)$ of the rotation-angle fluctuations for $\Delta\phi = 4^\circ$ and $\tau = 0.05$, as a function of ω and $\mathcal{C}$, for a time-discrete dynamical evolution of the photon polarisation (see Eq. (16)). The maximally correlated ($\mathcal{C} = 1$), white ($\mathcal{C} = 0$) and anticorrelated ($\mathcal{C} = -1$) noise regions are highlighted in blue, magenta and red, respectively. Plot (b): detail of the three noise spectral regions highlighted in plot (a), as a function of the noise frequency ω. Plot (c): measurement control spectrum $F(\omega)$ for $\Delta\phi = 4^\circ$ and $\tau = 0.05$, as a function of ω and θ, again in the time-discrete evolution case (see Eq. (17)).

strictly depends on the transmittance parameter θ.

Once again, it is worth noting that, in our setup (Fig. 2), the frequency domain for $G(\omega)$ and $F(\omega)$ is restricted to the interval $(-\pi/\tau, \pi/\tau)$, since the time evolution is discrete. Fig. 6a shows the behavior of $G(\omega)$ as a function of ω and the correlation coefficient $\mathcal{C}$, with Fig. 6b illustrating in detail the maximally correlated (in blue), anticorrelated (in red) and white noise (in magenta) cases, while Fig. 6c shows the dependence of $F(\omega)$ on ω and the measurement selective strength θ. In the figure, both $G(\omega)$ and $F(\omega)$ have been plotted for $\Delta\phi = 4^\circ$, as in our experimental implementation, and $\tau = 0.05$).

For *highly correlated* jumps ($\mathcal{C} \approx 1$) we find that

$$G(\omega) \approx \frac{\Delta\phi^2}{\pi\tau^2} \frac{\Gamma_{\rm B}}{\Gamma_{\rm B}^2 + \omega^2}, \tag{18}$$

i.e. $G(\omega)$ can be approximated by a narrow Lorentzian of width $\Gamma_{\rm B} = (1-\mathcal{C})/\tau$. In Fig. 6a one can observe how, for *partly correlated* random polarisation rotation jumps ($0 < \mathcal{C} < 1$), the peak shown by $G(\omega)$ at $\omega = 0$ decreases with $\mathcal{C}$, becoming also broader in the process.
For projective measurements ($\theta = 0$), $F(\omega)$ acquires the constant value $\tau/(2\pi)$, whereas for $\theta \neq 0$ $F(\omega)$ shows a peaked distribution centered at $\omega = 0$, with a characteristic width $\nu = [2\pi F(0)]^{-1}$. This indicates that the presence of projective measurements causes a *reduction* of the γ value, which is a signature of the QZE. However, the QZE signature disappears in the uncorrelated case $\mathcal{C} = 0$, which corresponds to a flat spectral density $G(\omega) = \Delta\phi^2/(2\pi\tau)$.
For *highly anticorrelated* jumps ($\mathcal{C} \approx -1$), instead, the bath spectrum $G(\omega)$ is a sum of two shifted narrow Lorentzians of width $\Gamma'_{\rm B} = (1+\mathcal{C})/\tau$, centered in $\omega = \pm\pi/\tau$, such that:

$$G(\omega) \approx \sum_{k=\pm 1} \frac{\Delta\phi^2}{\pi\tau^2} \frac{\Gamma'_{\rm B}}{{\Gamma'_{\rm B}}^2 + (\pi/\tau + k\omega)^2}. \tag{19}$$

In general $G(\omega)$ is peaked at $\omega = \pm\pi/\tau$ for anticorrelated consecutive polarisation-angle jumps ($-1 < \mathcal{C} < 0$), see Fig. 6a. Such anti-correlated polarisation rotation jumps correspond to the AZE trend, whereby γ increases with the measurement rate ν, as opposed to the QZE trend that is observed for correlated jumps.

DETAILED DESCRIPTION OF THE ITERATIVE PROCEDURE IN THE EXPERIMENTAL IMPLEMENTATION

Consider an iterative procedure in which a single photon, initialised in the horizontally-polarised state $|H\rangle$, passes through a sequence of N blocks at time instants $t_1, \ldots, t_N$. Without losing generality, let us choose as initial state $|\psi_{t_0}\rangle = |H\rangle$. In our experimental scheme, at the beginning of the k-th block, the state undergoes two polarisation rotations before the polariser (see Fig. 1). The first one is a (random) polarisation jump $U(\Delta\phi_k)$, while the second one is a counter-rotation $U(-\alpha_k)$ that, combined with the subsequent projection $|H\rangle\langle H|$, simulates the effect of the θ-dependent photon absorption induced by the (partially-)selective measurement

$$\Pi = |H\rangle\langle H| + \theta\,|V\rangle\langle V| = \theta I + (1-\theta)\,|H\rangle\langle H|, \tag{20}$$

with $\theta \in [0,1]$, at the k-th time instant t_k. At the end of the block, the projected single-photon state undergoes the rotation $U(\beta_k)$, in order to match the polarisation state entering the $(k+1)$-th block of our iterative protocol, i.e. the one obtained after k combined implementations of polarisation jump $U(\Delta\phi_k)$ and measurement Π. By properly choosing the $\{\alpha_k\}$ and $\{\beta_k\}$ sets, it is possible to recreate the dynamics induced on the single photon by a sequence of N blocks each performing a random polarisation rotation $U(\Delta\phi)$ followed by the partially-selective projector Π in Eq. (20). To do this, let us remind the reader that, at the k-th iteration, the survival probability $P_{\rm sur}^{(k)}$ of the entering polarisation state $|\psi_{t_k}\rangle = \cos\gamma_k\,|H\rangle + \sin\gamma_k\,|V\rangle$ is:

$$P_{\rm sur}^{(k)} = \prod_{n=1}^{k-1} P_{\rm sur}(n) \tag{21}$$

where $P_{\rm sur}(n)$ is the probability that the initial state survives after the n-th step. Then, the state $|\psi_{t_k}\rangle$ undergoes a phase shift $U(\Delta\phi_k)$ and the measurement Π, leading to the non-normalised state:

$$\Pi U(\Delta\phi_k)\,|\psi_{t_k}\rangle = \cos(\gamma_k + \Delta\phi_k)\,|H\rangle + \theta\sin(\gamma_k + \Delta\phi_k)\,|V\rangle \tag{22}$$

with corresponding survival probability

$$P_{\rm sur}(k) = \cos^2(\gamma_k + \Delta\phi_k) + \theta^2\sin^2(\gamma_k + \Delta\phi_k). \tag{23}$$

Therefore, the entering polarisation state at the $(k+1)$-th iteration is:

$$\left|\psi_{t_{k+1}}\right\rangle = \frac{\cos(\gamma_k + \Delta\phi_k)\,|H\rangle + \theta\sin(\gamma_k + \Delta\phi_k)\,|V\rangle}{\sqrt{P_{\rm sur}(k)}}. \tag{24}$$

In the proposed scheme (Fig. 1), by defining $\delta_k \equiv \gamma_k + \Delta\phi_k - \alpha_k$, the evolution of the polarisation state after the PBS and the rotation $U(\beta)$ can be summarised as:

$$U(-\alpha_k)U(\Delta\phi_k)\,|\psi_{t_k}\rangle \xrightarrow{|H\rangle\langle H|} \cos\delta_k\,|H\rangle \xrightarrow{U(\beta_k)}$$

$$\xrightarrow{U(\beta_k)} \cos\delta_k\,(\cos\beta_k\,|H\rangle + \sin\beta_k\,|V\rangle) \tag{25}$$

where β_k is the polarisation angle of $\left|\psi_{t_{k+1}}\right\rangle$, i.e. the state entering the $(k+1)$-th block, with respect to the horizontal plane. The normalisation condition for the state after the projection Π reads:

$$P_{\rm sur}(k) = \cos^2\delta_k\,. \tag{26}$$

Thus, by comparing Eqs. (23) and (26), one has:

$$\cos^2\delta_k = \cos^2(\gamma_k + \Delta\phi_k) + \theta^2\sin^2(\gamma_k + \Delta\phi_k)\,. \tag{27}$$

Using both Eq. (27) and the definition of δ_k, we can derive α_k as a function of the parameters γ_k, $\Delta\phi_k$ and θ.
Finally, to obtain the proper polarisation state $\left|\psi_{t_{k+1}}\right\rangle$, we implement the rotation $U(\beta_k)$, where β_k is implicitly given by the following relations:

$$\begin{cases} \cos\beta_k = \frac{\cos(\gamma_k+\Delta\phi_k)}{\cos\delta_k} \\ \\ \sin\beta_k = \frac{\theta\sin(\gamma_k+\Delta\phi_k)}{\cos\delta_k}\,. \end{cases} \tag{28}$$

Experimentally, we merged the rotations of subsequent half-wave plates by properly rotating a single one, reproducing their combined effect.

Demonstration of the consistency of Eq. (28) solutions

Here we demonstrate that Eq. (28) has always solution, as a further validation of our method. Let us rewrite equation system in Eq. (28) in the following way:

$$\begin{cases} \tan\beta_k = \theta\tan\Gamma_k \\ \\ \cos\delta_k = \frac{\cos\Gamma_k}{\cos\beta_k}\,, \end{cases} \tag{29}$$

with $\Gamma_k = \gamma_k + \Delta\phi_k$. While the first equation can always be solved, the second one has solution only for $|\cos\Gamma_k| \leq |\cos\beta_k|$. To show that this condition is always satisfied, let us write:

$$\Gamma'_k = \Gamma_k - n\pi, \qquad n: \;\; \Gamma'_k \in \left(-\frac{\pi}{2}, \frac{\pi}{2}\right]. \tag{30}$$

Substituting it in Eq. (29), one obtains

$$\begin{cases} \tan\beta_k = \theta\tan\Gamma'_k \\ \\ \cos\delta_k = (-1)^n\frac{\cos\Gamma'_k}{\cos\beta_k}\,, \end{cases} \tag{31}$$

Assuming $\beta_k \in (-\frac{\pi}{2}, \frac{\pi}{2}]$, and considering that $\theta \in [0,1]$, by taking the absolute value of both sides of the upper equation in system (31) one has:

$$\tan|\beta_k| = \theta\tan|\Gamma'_k| \leq \tan|\Gamma'_k|\,. \tag{32}$$

Since $\tan\phi$ is a monotone increasing function for $\phi \in (-\frac{\pi}{2}, \frac{\pi}{2}]$, inequality (32) implies for $\beta_k, \Gamma'_k \in (-\frac{\pi}{2}, \frac{\pi}{2}]$ (i.e. in our case):

$$|\beta_k| \leq |\Gamma'_k|\,. \tag{33}$$

If we take the absolute value of both sides of the bottom equation in system (31), this leads to write:

$$|\cos\delta_k| = \left|\frac{\cos\Gamma'_k}{\cos\beta_k}\right| = \frac{\cos|\Gamma'_k|}{\cos|\beta_k|} \leq 1\,, \tag{34}$$

where the last inequality follows from Eq. (33), considering that $\cos\phi$ is non-negative for $\phi \in (-\frac{\pi}{2}, \frac{\pi}{2}]$ and decreasing for $\phi \in (0, \frac{\pi}{2}]$.
By proving this inequality, we can state that both the equations present in Eq. (28) can always be solved, demonstrating the robustness of our procedure and its corresponding experimental implementation.

ANALYSIS OF THE METHOD ROBUSTNESS WITH RESPECT TO A GENERAL UNITARY POLARIZATION NOISE PROCESS

In the following, we will show the results of the numerical simulations performed by applying our noise sensing technique to a more general noise model, i.e., an arbitrary unitary polarization noise process. Specifically, for each of the k-th time instant t_k of our protocol ($k = 1, ..., N$) we consider a generic rotation on a random axis of the Bloch sphere:

$$U_{\vec{n}_k}(\Delta\phi_k) = I\cos(\Delta\phi_k) - i(\vec{n}_k \cdot \vec{\sigma})\sin(\Delta\phi_k), \tag{35}$$

being $\vec{n}_k = \{n_1^{(k)}, n_2^{(k)}, n_3^{(k)}\}$ a unit vector in the Bloch sphere and $\vec{\sigma} = \{\sigma_x, \sigma_y, \sigma_z\}$ the Pauli matrices vector. In this particular scenario, the correlation coefficient $\mathcal{C}$ among the noise contributions (see Eq. (5)) is evaluated as the average scalar product between the unit vectors determining the Bloch sphere axes of subsequent polarization rotations (the overline indicates the averaging operation)

$$\mathcal{C} = \overline{\vec{n}_{k+1} \cdot \vec{n}_k}. \tag{36}$$

For the sake of generality, instead of considering a polarization jump with fixed magnitude like in the theoretical model previously illustrated (i.e., putting $|\Delta\phi_k| = \Delta\phi = 4^\circ$), we also take into account a randomly varying rotation angle $\Delta\phi_k$. To have a quantitative estimation of the reliability of our method against different levels of noise, we perform our analysis by randomly choosing $\Delta\phi_k$ within three different intervals, namely $[\Delta\phi/2, 3\Delta\phi/2]$, $[0, 2\Delta\phi]$ and $[-\Delta\phi, 3\Delta\phi]$, still maintaining the same average rotation jump.

The simulations results are reported in Fig. 7 for the correlated case ($\mathcal{C} = 0.4$), Fig. 8 for the uncorrelated case ($\mathcal{C} = 0$) and Fig. 9 for the anti-correlated case ($\mathcal{C} = -0.6$). As expected, if we consider the general case of polarization rotations occurring around a random axis of the Bloch sphere, but with a fixed amplitude $\Delta\phi$, we find a situation similar to what obtained in our experiment. In fact, by comparing plots (b)-(d) of Fig. 3 with Fig. 7a, Fig. 8a and 9a, respectively, we can appreciate how, both for the general case and the simplified model considered for our experiment, the QZE (AZE) can be observed in case of (anti-)correlated noise, while the two data sets initially overlap for Markovian noise. The only noticeable difference between the fixed and random axis polarization rotation is the slightly smaller separation between the orange and blue data sets for the latter, due to the fact that, in each step, the polarization rotation component along the z-axis (the one on which we perform our polarization measurements) is, of course, lesser or equal to the one of the former case. If we then randomize not just the polarization rotation axis, but also the rotation amplitude $\Delta\phi$, plots (b)-(d) of Figs. 7-9 show us how the (anti-)Zeno dynamics, although decreasing in magnitude as the $\Delta\phi$ values spectrum grows, can still be associated with (anti-)correlated noise. This happens even for heavily fluctuating rotation amplitude, shown in Figs. 7d, 8d and 9d, in which the $\Delta\phi$ of each step can be randomly chosen in the wide interval $[-\Delta\phi, 3\Delta\phi]$, including values even departing from the small $\Delta\phi$ scenario considered for the experimentally tested model. By looking at these plots, we can appreciate the extreme robustness and reliability of our method in identifying whether the polarization rotation noise present in our quantum channel is (anti-)correlated, even beyond the small fluctuations limit. Furthermore, if we observe the behavior of the quantity $\Delta\overline{P}_H(t_k) = \overline{P}_H^{\theta=0}(t_k) - \overline{P}_H^{\theta=1}(t_k)$, being $\overline{P}_H^{\theta=0}(t_k)$ and $\overline{P}_H^{\theta=1}(t_k)$ the average probabilities of detecting a horizontally-polarized photon at the time instant t_k with or without Zeno-like measurements, respectively, we can notice how this quantity could be the key to a quantitative estimation of both the degree of correlation of the noise and the variability of its intensity (we leave this aspect to further investigations). Hence, the results of our proof-of-principle experiment, although obtained considering a simplified polarization noise model, still hold for the general case addressed by our numerical simulations.
These results point out that our diagnostic method can be extended to very general classes of noise. Anyway, the precise implementation of this scheme is demanded to future investigation.

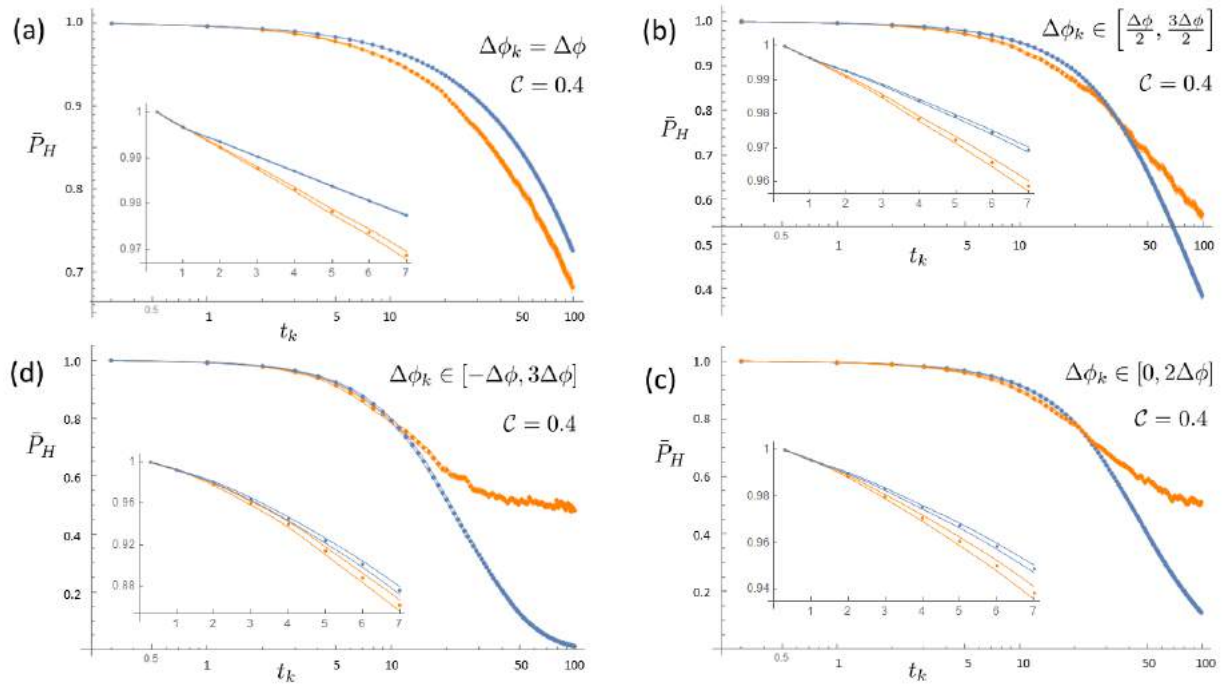

FIG. 7. Numerical simulations, obtained by averaging over 1000 simulated random sequences the quantity in Eq. (4), estimating the performance of our QZE/AZE-based method for highlighting (anti-)correlated noise in the case of a random polarization rotation. Panels (a-d): theoretical average probability $\bar{P}_H(t_k)$ to detect a horizontally-polarised single photon for correlated subsequent rotations in the whole Bloch sphere ($\mathcal{C} = 0.4$, evaluated following Eq. (36)), as a function of t_k. The magnitude of each step rotation is $\Delta\phi_k = \Delta\phi = 4^\circ$ for plot (a), like in our experimental implementation. In the remaining three plots, $\Delta\phi_k$ is randomly chosen in the intervals $[\Delta\phi/2, 3\Delta\phi/2]$ (plot (b)), $[0, 2\Delta\phi]$ (plot (c)), $[-\Delta\phi, 3\Delta\phi]$ (plot (d)). The orange dots illustrate the behavior in the absence of measurement, while the case of Zeno-like projective measurements is shown by the blue dots. The orange and blue lines indicate, respectively, the estimated statistical uncertainties on the simulated data. The inset plots show the detail of the experimentally-investigated region $t_k \in [0, 7]$.

[1] H. M. Wiseman and G. J. Milburn, *Quantum Measurement and Control* (Cambridge University Press, 2009).
[2] C. Brif, R. Chakrabarti, and H. Rabitz, Control of quantum phenomena: past, present and future, New J. Phys. **12**, 075008 (2010).
[3] B. Misra and E. C. G. Sudarshan, The Zeno's paradox in quantum theory, J. of Math. Phys. **18**, 756 (1977).
[4] W. M. Itano, D. J. Heinzen, J. J. Bollinger, and D. J. Wineland, Quantum Zeno effect, Phys. Rev. A **41**, 2295 (1990).
[5] A. G. Kofman and G. Kurizki, Quantum Zeno effect on atomic excitation decay in resonators, Phys. Rev. A **54**, R3750 (1996).
[6] D. Home and M. Whitaker, A conceptual analysis of quantum zeno; paradox, measurement, and experiment, Annals of Physics **258**, 237 (1997).
[7] K. Koshino and A. Shimizu, Quantum zeno effect by general measurements, Physics Reports **412**, 191 (2005).
[8] K. Thapliyal, A. Pathak, and J. Peřina, Linear and nonlinear quantum zeno and anti-zeno effects in a nonlinear optical coupler, Phys. Rev. A **93**, 022107 (2016).
[9] A. G. Kofman and G. Kurizki, Acceleration of quantum decay processes by frequent observations, Nature **405**, 546 (2000).
[10] P. Facchi, H. Nakazato, and S. Pascazio, From the quantum zeno to the inverse quantum zeno effect, Phys. Rev. Lett. **86**, 2699 (2001).
[11] M. Yamaguchi, T. Asano, and S. Noda, Photon emission by nanocavity-enhanced quantum anti-zeno effect in solid-state cavity quantum-electrodynamics, Opt. Express **16**, 18067 (2008).
[12] M. C. Fischer, B. Gutiérrez-Medina, and M. G. Raizen, Observation of the quantum Zeno and anti-Zeno effects in an unstable system, Phys. Rev. Lett. **87**, 040402 (2001).
[13] P. Facchi and S. Pascazio, Quantum Zeno subspaces, Phys. Rev. Lett. **89**, 080401 (2002).
[14] F. Schäfer, I. Herrera, S. Cherukattil, C. Lovecchio, F. S. Cataliotti, F. Caruso, and A. Smerzi, Experimental realization of quantum Zeno dynamics, Nat. Commun. **5**, 3194 (2014).
[15] A. Signoles, A. Facon, D. Grosso, I. Dotsenko, S. Haroche, J.-M. Raimond, M. Brune, and S. Gleyzes, Confined quantum Zeno dynamics of a watched atomic arrow, Nat. Phys. **10**, 715 (2014).
[16] S. Gherardini, S. Gupta, F. S. Cataliotti, A. Smerzi, F. Caruso, and S. Ruffo, Stochastic quantum Zeno by large deviation theory, New J. Phys. **18**, 013048 (2016).
[17] M. M. Müller, S. Gherardini, and F. Caruso, Stochastic quantum Zeno-based detection of noise correlations, Sci. Rep. **6**, 38650 (2016).
[18] P. Facchi and S. Pascazio, Quantum zeno dynamics: mathematical and physical aspects, Journal of Physics A: Mathematical and Theo-

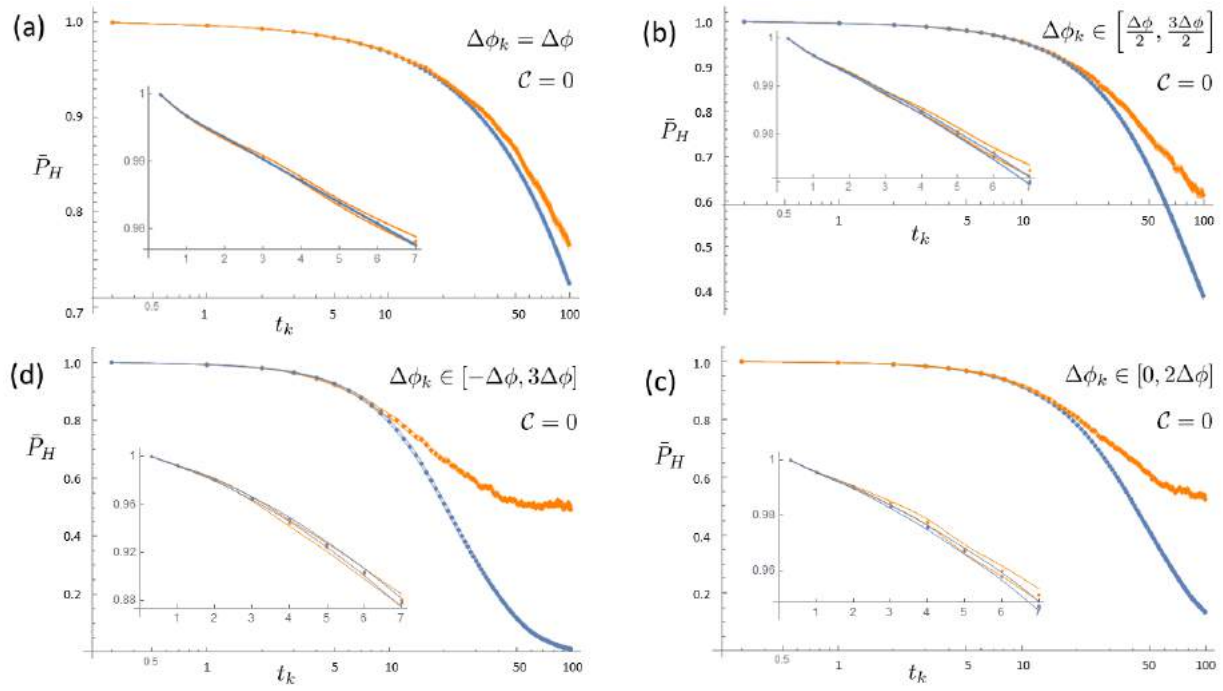

FIG. 8. Numerical simulations, obtained by averaging over 1000 simulated random sequences the quantity in Eq. (4), estimating the performance of our QZE/AZE-based method for highlighting (anti-)correlated noise in the case of a random polarization rotation. Panels (a-d): theoretical average probability $\bar{P}_H(t_k)$ to detect a horizontally-polarised single photon for uncorrelated subsequent rotations in the whole Bloch sphere ($\mathcal{C} = 0$, evaluated following Eq. (36)), as a function of t_k. The magnitude of each step rotation is $\Delta\phi_k = \Delta\phi = 4^\circ$ for plot (a), like in our experimental implementation. In the remaining three plots, $\Delta\phi_k$ is randomly chosen in the intervals $[\Delta\phi/2, 3\Delta\phi/2]$ (plot (b)), $[0, 2\Delta\phi]$ (plot (c)), $[-\Delta\phi, 3\Delta\phi]$ (plot (d)). The orange dots illustrate the behavior in the absence of measurement, while the case of Zeno-like projective measurements is shown by the blue dots. The orange and blue lines indicate, respectively, the estimated statistical uncertainties on the simulated data. The inset plots show the detail of the experimentally-investigated region $t_k \in [0, 7]$.

retical **41**, 493001 (2008).
[19] P. G. Kwiat, A. G. White, J. R. Mitchell, O. Nairz, G. Weihs, H. Weinfurter, and A. Zeilinger, High-efficiency quantum interrogation measurements via the quantum zeno effect, Phys. Rev. Lett. **83**, 4725 (1999).
[20] H. Zheng, S. Y. Zhu, and M. S. Zubairy, Quantum zeno and anti-zeno effects: Without the rotating-wave approximation, Phys. Rev. Lett. **101**, 200404 (2008).
[21] M. M. Müller, S. Gherardini, and F. Caruso, Quantum Zeno dynamics through stochastic protocols, Ann. Phys. **529**, 1600206 (2017).
[22] A. G. Kofman and G. Kurizki, Universal dynamical control of quantum mechanical decay: Modulation of the coupling to the continuum, Phys. Rev. Lett. **87**, 270405 (2001).
[23] L. Zhou, S. Yang, Y.-x. Liu, C. P. Sun, and F. Nori, Quantum zeno switch for single-photon coherent transport, Phys. Rev. A **80**, 062109 (2009).
[24] S. Hacohen-Gourgy, L. P. García-Pintos, L. S. Martin, J. Dressel, and I. Siddiqi, Incoherent qubit control using the quantum zeno effect, Phys. Rev. Lett. **120**, 020505 (2018).
[25] A. Pechen, N. Il'in, F. Shuang, and H. Rabitz, Quantum control by von neumann measurements, Phys. Rev. A **74**, 052102 (2006).
[26] J. J. W. H. Sørensen, M. Dalgaard, A. H. Kiilerich, K. Mølmer, and J. F. Sherson, Quantum control with measurements and quantum zeno dynamics, Phys. Rev. A **98**, 062317 (2018).
[27] S. Maniscalco, F. Francica, R. L. Zaffino, N. Lo Gullo, and F. Plastina, Protecting entanglement via the quantum zeno effect, Phys. Rev. Lett. **100**, 090503 (2008).
[28] F. Piacentini, A. Avella, E. Rebufello, R. Lussana, F. Villa, A. Tosi, M. Gramegna, G. Brida, E. Cohen, L. Vaidman, I. P. Degiovanni, and M. Genovese, Determining the quantum expectation value by measuring a single photon, Nat. Phys. **13**, 1191 (2017).
[29] G. A. Paz-Silva, A. T. Rezakhani, J. M. Dominy, and D. A. Lidar, Zeno effect for quantum computation and control, Phys. Rev. Lett. **108**, 080501 (2012).
[30] X.-B. Wang, J. Q. You, and F. Nori, Quantum entanglement via two-qubit quantum zeno dynamics, Phys. Rev. A **77**, 062339 (2008).
[31] G. Barontini, L. Hohmann, F. Haas, J. Estève, and J. Reichel, Deterministic generation of multiparticle entanglement by quantum zeno dynamics, Science **349**, 1317 (2015).
[32] A. G. Kofman, G. Kurizki, and T. Opatrný, Zeno and anti-Zeno effects for photon polarization dephasing, Phys. Rev. A **63**, 042108 (2001).
[33] A. G. Kofman and G. Kurizki, Unified theory of dynamically suppressed qubit decoherence in thermal baths, Phys. Rev. Lett. **93**, 130406 (2004).

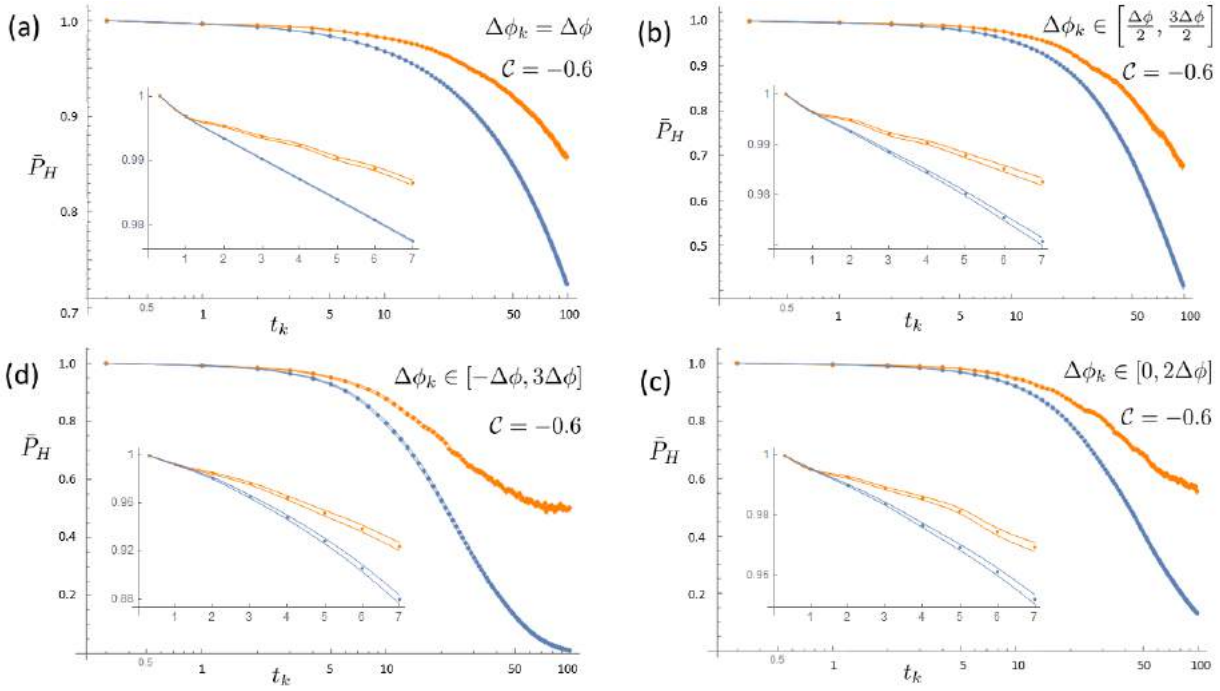

FIG. 9. Numerical simulations, obtained by averaging over 1000 simulated random sequences the quantity in Eq. (4), estimating the performance of our QZE/AZE-based method for highlighting (anti-)correlated noise in the case of a random polarization rotation. Panels (a-d): theoretical average probability $\bar{P}_H(t_k)$ to detect a horizontally-polarised single photon for anti-correlated subsequent rotations in the whole Bloch sphere ($\mathcal{C} = -0.6$, evaluated following Eq. (36)), as a function of t_k. The magnitude of each step rotation is $\Delta\phi_k = \Delta\phi = 4^\circ$ for plot (a), like in our experimental implementation. In the remaining three plots, $\Delta\phi_k$ is randomly chosen in the intervals $[\Delta\phi/2, 3\Delta\phi/2]$ (plot (b)), $[0, 2\Delta\phi]$ (plot (c)), $[-\Delta\phi, 3\Delta\phi]$ (plot (d)). The orange dots illustrate the behavior in the absence of measurement, while the case of Zeno-like projective measurements is shown by the blue dots. The orange and blue lines indicate, respectively, the estimated statistical uncertainties on the simulated data. The inset plots show the detail of the experimentally-investigated region $t_k \in [0, 7]$.

[34] J. Clausen, G. Bensky, and G. Kurizki, Bath-optimized minimal-energy protection of quantum operations from decoherence, Phys. Rev. Lett. **104**, 040401 (2010).

[35] P. M. Harrington, J. T. Monroe, and K. W. Murch, Quantum zeno effects from measurement controlled qubit-bath interactions, Phys. Rev. Lett. **118**, 240401 (2017).

[36] P. Biagioni, G. Della Valle, M. Ornigotti, M. Finazzi, L. Duò, P. Laporta, and S. Longhi, Experimental demonstration of the optical Zeno effect by scanning tunneling optical microscopy, Opt. Express **16**, 3762 (2008).

[37] N. Erez, G. Gordon, M. Nest, and G. Kurizki, Thermodynamic control by frequent quantum measurements, Nature **452**, 724 (2008).

[38] G. A. Álvarez, D. D. B. Rao, L. Frydman, and G. Kurizki, Zeno and anti-Zeno polarization control of spin ensembles by induced dephasing, Phys. Rev. Lett. **105**, 160401 (2010).

[39] G. Gordon and G. Kurizki, Universal dephasing control during quantum computation, Phys. Rev. A **76**, 042310 (2007).

[40] A. Zwick, G. A. Álvarez, and G. Kurizki, Maximizing information on the environment by dynamically controlled qubit probes, Phys. Rev. Applied **5**, 014007 (2016).

[41] C. O. Bretschneider, G. A. Álvarez, G. Kurizki, and L. Frydman, Controlling spin-spin network dynamics by repeated projective measurements, Phys. Rev. Lett. **108**, 140403 (2012).

[42] H.-V. Do, C. Lovecchio, I. Mastroserio, N. Fabbri, F. S. Cataliotti, S. Gherardini, M. M. Müller, N. Dalla Pozza, and F. Caruso, Experimental proof of quantum Zeno-assisted noise sensing, New J. Phys. **21**, 113056 (2019).

[43] M. M. Müller, S. Gherardini, N. Dalla Pozza, and F. Caruso, Noise sensing via stochastic quantum Zeno, Phys. Lett. A **384**, 126244 (2020).

[44] M. O. Scully and M. S. Zubairy, *Quantum Optics* (Cambridge University Press, 1997).

[45] B. Tamir and E. Cohen, Introduction to weak measurements and weak values, Quanta **2**, 7 (2013).

[46] G. J. Milburn, Quantum Zeno effect and motional narrowing in a two-level system, J. Opt. Soc. Am. B **5**, 1317 (1988).

[47] A. Peres and A. Ron, Incomplete "collapse" and partial quantum Zeno effect, Phys. Rev. A **42**, 5720 (1990).

[48] B. Sephton, A. Dudley, G. Ruffato, F. Romanato, L. Marrucci, M. Padgett, S. Goyal, F. Roux, T. Konrad, and A. Forbes, A versatile quantum walk resonator with bright classical light, PLoS ONE **14**, e0214891 (2019).

[49] C. Benedetti, M. G. A. Paris, and S. Maniscalco, Non-Markovianity of colored noisy channels, Phys. Rev. A **89**, 012114 (2014).

[50] R. B. Wu, T. F. Li, A. G. Kofman, J. Zhang, Y.-X. Liu, Y. A. Pashkin, J.-S. Tsai, and F. Nori, Spectral analysis and identification of noises in quantum systems, Phys. Rev. A **87**, 022324 (2013).

[51] S. Banerjee, J. Naikoo, and R. Srikanth, Distinguishing environment-induced non-Markovianity from subsystem dynamics, Int. J. Quan-

tum Inf. **18**, 2050042 (2020).
[52] D. Goldring, Z. Zalevsky, G. Shabtay, D. Abraham, and D. Mendlovic, Magneto-optic-based devices for polarization control, J. Opt. A **6**, 98 (2003).
[53] X. S. Yao, L. Yan, and Y. Shi, Highly repeatable all-solid-state polarization-state generator, Opt. Lett. **30**, 1324 (2005).
[54] L. Chen and W. She, Arbitrary-to-linear or linear-to-arbitrary polarization controller based on Faraday and Pockels effects in a single BGO crystal, Opt. Express **15**, 15589 (2007).
[55] T. Saitoh and S. Kinugawa, Magnetic field rotating-type Faraday polarization controller, IEEE Photon. Technol. Lett. **15**, 1404 (2003).
[56] M. J. D. Macpherson, K. P. Zetie, R. B. Warrington, D. N. Stacey, and J. P. Hoare, Precise measurement of parity nonconserving optical rotation at 876 nm in atomic bismuth, Phys. Rev. Lett. **67**, 2784 (1991).
[57] A. H. Gevorgyan, M. Z. Harutyunyan, S. A. Mkhitaryan, E. A. Santrosyan, and G. A. Vardanyan, A polarization amplifier and stabilizer based on Fabri–Perot resonator filled with chiral photonic crystal, Optik **121**, 39 (2010).
[58] D. M. Meekhof, P. Vetter, P. K. Majumder, S. K. Lamoreaux, and E. N. Fortson, High-precision measurement of parity nonconserving optical rotation in atomic lead, Phys. Rev. Lett. **71**, 3442 (1993).
[59] M. Leonetti, L. Pattelli, S. De Panfilis, D. S. Wiersma, and G. Ruocco, Spatial coherence of light inside three-dimensional media, Nat. Commun. **12**, 4199 (2021).
[60] M. M. Zakharova, V. A. Nasonova, A. F. Konstantinova, V. S. Chudakov, and R. V. Gaĭnutdinov, An investigation of the optical properties of cholesterol crystals in human synovial fluid, Crystallogr. Rep. **54**, 509 (2009).
[61] M. W. Ropes and W. Bauer, Synovial fluid changes in joint disease, J. Bone Jt. Surg. **36** (1954).
[62] W. H. R. Nye, R. Terry, and D. L. Rosenbaum, Two Forms of Crystalline Lipid in "Cholesterol" Effusions, Am. J. Clin. Pathol. **49**, 718 (1968).
[63] M. Kashiwagi, L. Liu, K. K. Chu, C.-H. Sun, A. Tanaka, J. A. Gardecki, and G. J. Tearney, Feasibility of the assessment of cholesterol crystals in human macrophages using micro optical coherence tomography, PLoS One **9**, 1 (2014).
[64] L. Whitmore and B. A. Wallace, Protein secondary structure analyses from circular dichroism spectroscopy: methods and reference databases, Biopolymers **89**, 392 (2008).
[65] A. J. Miles and B. A. Wallace, Circular dichroism spectroscopy of membrane proteins, Chem. Soc. Rev. **45**, 4859 (2016).